# INFLUENCE OF TRANSFORMATION TEMPERATURE ON CARBIDE PRECIPITATION SEQUENCE DURING LOWER BAINITE FORMATION

F.G. Caballero[1], M.K. Miller[2] and C. Garcia-Mateo[1]

[1] Centro Nacional de Investigaciones Metalúrgicas (CENIM-CSIC), Avda. Gregorio del Amo, 8. E-28040 Madrid, Spain

[2] Oak Ridge National Laboratory (ORNL), Materials Science and Technology Division; P.O. Box 2008, Oak Ridge, TN 37831-6139, USA

Corresponding Author:

F.G. Caballero

Tlf: +34 91 553 89 00 (Ext 373)

Fax +34 91 534 7425

E-mail: fgc@cenim.csic.es

**Abstract**

The nature of different carbides formed during the lower bainite reaction at different transformation temperatures was determined by atom probe tomography in three steels with different carbon and silicon contents. It is known that steel composition and temperature alter the carbide precipitation sequence during low-temperature bainite

formation. However, present results confirm that dislocations in lower bainite that are more prominent at the lower the transformation temperature, trap a substantial amount of carbon and hence, can influence the carbide precipitation sequence and, in particular, can determine where ε-carbide forms before the growth of cementite.

Keywords: carbides, precipitation, tomography, metals

## Introduction

The difference in carbide distribution between bainite formed at high and low temperatures, viz., interlath and intralath, respectively, appears to exist in a majority of steels and makes the classical nomenclature of upper and lower bainite useful in describing the appearance of the microstructure. The precipitation of carbides during the bainite reaction is a secondary process, not essential to the mechanism of formation of bainitic ferrite, except where any precipitation influences the reaction rate by removing carbon either from the residual austenite or from the supersaturated ferrite [1,2]. In upper bainite, the carbides precipitate from the carbon-enriched residual austenite between the developing laths. Thus, upper bainitic ferrite itself is generally free from intralath precipitates. In contrast, many observations reveal that lower bainitic cementite nucleates and grows within supersaturated bainitic ferrite in a process identical to the tempering of martensite [3]. The slower diffusion associated with the reduced transformation temperature provides an opportunity for some of the carbon to precipitate in the supersaturated bainitic ferrite. A fine dispersion of plate-like carbides is then found inside the bainitic ferrite, which also has a plate morphology, with a single

crystallographic variant within a given bainitic ferrite plate, although it is possible to observe more than one variant of carbide precipitation in a lower bainite sub-unit [3,4].

Matas and Hehemann [5] first suggested that the initial carbide in lower bainite is ε-carbide, which is subsequently dissolved and replaced by cementite. The rate at which the ε-carbide converts to cementite increases with the temperature, but also depends on the steel composition. In fact, a high silicon concentration retards the reaction, as is commonly observed in the tempering of martensite [6-11]. Owen [8] proposed that silicon rejected from cementite acts as a growth barrier and causes the inhibition of cementite precipitation. Since then, partitioning of silicon between cementite and ferrite has attracted considerable attention [12-15].

The detection of ε-carbide instead of cementite in lower bainite implies the existence of a significant amount of carbon in super-saturation in bainitic ferrite [16]. However, ε-carbide is not always found as a precursor to the precipitation of cementite in lower bainite. Bhadeshia and Edmonds [17] failed to detect ε-carbide in a high silicon medium carbon steel even during the early stages of the lower bainite transformation.

Kozeschnik and Bhadeshia [18] utilised theory of the kinetics of precipitation and provided a quantitative framework for the formation of cementite from supersaturated ferrite. They conducted calculations for the so-called *4340* steel with a chemical composition of Fe-0.4C-0.7Mn-0.28Si-0.8Cr–-.8Ni-0.25Mo (wt.%) and the alloy 300M with essentially the same composition, but with the silicon concentration increased to 1.6 wt.%. The *4340* steel is a high strength steel used in the quenched and tempered condition that exhibits tempered martensite embrittlement at 350 ºC [19]. Tempered martensite embrittlement is associated with the formation of coarse cementite, which dramatically reduces toughness in a high strength matrix. By contrast, alloy 300M with

a higher silicon concentration, added to retard the para-equilibrium precipitation of cementite, can be tempered at just 315 ºC without embrittlement, leading to a much greater toughness.

Calculations by Ghosh and Olson [20] suggested, however, that precipitation is too rapid to have a perceptible effect of silicon. Kozeschnik and Bhadeshia's calculations [18] on the kinetics of cementite precipitation from supersaturated ferrite confirmed that the cementite precipitates rapidly during tempering at 315 ºC, with little meaningful difference between the silicon enriched 300M and low silicon 4340 steels. One probable explanation for the discrepancy between calculations [18,20] and experimental observations on the tempering of martensite comes from earlier classic work by Kalish and Cohen [21]. They proposed that in the presence of dislocations, carbon prefers to segregate to dislocations rather than precipitate as cementite or ε-carbide.

Defects can effectively be thought of as a separate trapping site, which is a greater attractor for carbon than cementite. In these circumstances, the carbon available for precipitation as cementite is reduced. The rate of precipitation then depends on the removal of defects during annealing, making carbon available for cementite formation [22]. This process must greatly retard tempering kinetics and, because of the reduced carbon concentration in the perfect lattice, lead to a smaller driving force for precipitation and hence, a larger difference between the silicon-enriched and low-silicon steels.

In the present work, the nature of the iron carbides formed during lower bainite reaction was determined by atom probe tomography (APT) in steels transformed over a wide range of temperatures (200-425 ºC). In addition, carbon trapping at dislocations was

analyzed to elucidate the role of defects altering the carbide precipitation sequence during lower bainite formation.

The carbon concentration of precipitates obtained from APT was used to discriminate amongst ε-carbide ($Fe_{2.4}C$ with ~30 at.% C), cementite ($Fe_3C$ with ~25 at.% C), and other iron transition carbides, such as $Fe_4C$ with ~20 at.% C and $Fe_8C$ with ~11 at.% C. Previous work [23,24] focused on the analysis of iron carbides during tempering of a high-carbon, high-silicon bainitic steel, and the redistribution of substitutional solute across the carbide/ferrite interface, with special attention given to silicon. The goal of this study is to examine the carbide precipitation during lower bainite reaction at different temperatures in three steels with different carbon and silicon contents.

**Materials and Experimental Procedure**

Three steels with different carbon and silicon contents were selected to study the precipitation of carbides during bainite transformation at different temperatures. The bainite transformation temperature range of the steel is mainly a consequence of the carbon content, whereas silicon is known to retard cementite precipitation [8] due to its extremely low solubility in the cementite crystal structure. It is expected that the presence of silicon will depress the formation temperature of lower bainite since silicon prolongs the time needed for carbide precipitation. The alloys also contain Mn, Ni, V, Cr, and Mo for hardenability. The chemical composition of the steels is given in Table 1.

The medium-carbon and low-silicon (MC-LSi) steel was supplied as 30 mm hot rolled square bar; the medium-carbon and high-silicon (MC-HSi) steel was supplied as 12 mm hot rolled strips; the high-carbon and high-silicon (HC-HSi) steel was supplied as as-

cast ingots after homogenization at 1200 ºC for 48 h. Further details about the alloying design and manufacturing processes can be found elsewhere [25-27].

Dilatometric and metallographic analyses were used to determine the transformation temperatures in the selected steels. An Adamel Lhomargy DT1000 high-resolution dilatometer was used [28]. Cylindrical dilatometric test pieces of 3 mm in diameter and 12 mm in length were austenitised at the temperatures listed in Table 2, cooled down at 100 ºC/s to bainite transformation temperatures ranging from 200 to 525 ºC and then isothermally holding for different times to ensure complete transformation (see Table 3) before quenching to room temperature at a rate of 100 ºC/s.

The martensite start temperatures ($M_S$) listed in Table 2 were estimated by dilatometry. Dilatometric specimens were austenised using a heating rate of 5 ºC/s and then rapidly cooled at rate of 100ºC/s. Each test was performed twice. The formation of martensite during cooling was detected by monitoring the fractional change in dilatation with temperature.

Conventional metallographic examination by Light Optical Microscopy (LOM) and Scanning Electron Microscopy (SEM) was used to determine the bainite start temperatures ($B_S$) that are shown in Table 2. A JEOL model JSM-6500F Field Emission SEM operated at 7 kV was used for this purpose.

Transmission Electron Microscopy (TEM) specimens were made from disks that were cut from 3-mm-diameter rods and electropolished with a twin-jet electropolisher at room temperature in a mixture of 5% perchloric acid, 15% glycerol, and 80% methanol at 40 V until perforation occurred. A JEOL model JEM-2010 TEM was used to examine the carbide distribution, inter-lath and intra-lath, in the bainitic microstructure, and to identify the different morphologies of bainite, upper bainite, and lower bainite. The

observation of both inter- and intra-lath carbide distributions in the same bainitic microstructure enabled the transition temperatures ($LB_S$) from upper to lower bainite listed in Table 2 to be determined.

Specimens for APT were cut from the heat treated dilatometric samples and electropolished with the standard double layer and micropolishing methods [29]. Atom probe analyses were performed in the Oak Ridge National Laboratory (ORNL) local electrode atom probes (Cameca Instruments LEAP 2017 and LEAP 4000X HR). The local electrode atom probes were operated in voltage-pulse mode with a specimen temperature of 60 K, a pulse repetition rate of 200 kHz, and a pulse fraction of 0.2. The concentration of carbon is determining counting the number of carbon atoms in small slices perpendicular to one of the axes of the selected volume. The size of the slices is a compromise between maximizing the number of ion atoms and the spatial resolution. Error bars for APT values represent the statistical scatter in the composition profiles due to the number of ions in each slice of the selected volume of analysis.

**Results and Discussion**

The difference in carbide distribution, intra-lath and inter-lath, respectively, allows identifying both upper and lower bainite morphologies, as illustrated in Fig. 1. In upper bainite, the carbides precipitate from carbon-enriched residual austenite between bainitic ferrite laths. Inter-lath precipitation was observed in the MC-LSi steel after isothermal transformation at temperatures ranging from 475-525 ºC (Table 3). Upper bainitic ferrite ($\alpha$) itself is free from precipitates, as illustrated in Fig. 1a.

In contrast, carbides were mainly identified inside the ferrite laths in the MC-LSi steel after isothermal transformation at temperatures ranging from 375-425 ºC (Table 3). The

lower bainitic microstructure formed at 375 ºC in the MC-LSi steel is shown in Fig. 1b. Mixed microstructures of upper and lower bainite were observed after isothermal transformation at 450 ºC in the MC-LSi steel (Table 3). This difference is because the carbon enrichment of the austenite caused by upper bainite transformation can result in the subsequent formation of lower bainite [2]. The observation of a mixed carbide distribution allowed for defining the lower bainite start temperature (Table 2).

Silicon additions can prevent the precipitation of carbides between the laths of bainitic ferrite (i.e., upper bainite is carbide-free in high Si steels). A typical carbide-free bainitic microstructure after isothermal transformation at 425 ºC in the MC-HSi steel is displayed elsewhere [30], where it is possible to observe the subunits of bainitic ferrite with retained austenite ($\gamma$) between them. However, silicon does not have a significant effect on the precipitation of carbides inside the ferrite laths, as illustrated in Fig. 1c. Thus, the formation of lower bainite is not inhibited in the MC-HSi steel at temperatures ranging from 325-375 ºC (Table 3). Mixed microstructures of carbide-free and lower bainite were observed after isothermal transformation at 400 ºC in the MC-HSi steel (Table 3).

Remarkably, the image shown in Fig. 1d failed to reveal carbide particles inside the bainitic ferrite after transformation at 250 ºC in the HC-HSi steel, leading to the doubtful hypothesis that upper bainite was formed at this extremely low temperature. After extensive aging at 200 ºC for 14 days in the same steel, just a few 20 nm wide and 175 nm long cementite particles were observed by TEM inside a thicker bainitic ferrite plate [27]. The presence of intra-lath cementite as the lower bainite carbide in the HC-HSi steel was confirmed by APT after isothermal transformation at 200 and 300 ºC [31].

TEM examination also revealed that the growth of bainite is accompanied by the formation of dislocations in and around the bainitic ferrite as shown in Fig. 1e. Dislocation debris in the different bainitic microstructures is evident in both the bainitic ferrite and in the surrounding austenite. As in the case of martensite, the formation of bainite leads to a shape change in the transformed region. As bainitic transformation takes place at a temperature at which the shape change cannot be accommodated elastically, the plastic deformation that is driven by the shape change causes the accumulation of dislocations, which increase in number as the transformation temperature decreases [17,32].

The average carbon contents of different carbides formed during the lower bainite reaction at different transformation temperatures (200-425 ºC) and times long enough to ensure complete transformation in the studied steels (see Table 3 for details) were estimated from APT data with the use of concentration profiles across carbide-ferrite interfaces; the results are shown in Fig. 2. Examples of a carbon atom map showing carbon segregation across different carbide particles are shown in Figs. 3-5. Based on the carbon content, the different types of carbides detected were as follows:

i) Small features enriched in carbon and randomly dispersed throughout the bainitic ferrite matrix with a carbon content of 7-16 at. % C and without clear evidence of substitutional solute partitioning (Fig. 3). Only, solute such Mn seems to increase as a function of distance as the cluster is approached in Fig. 3. However, the statistical scatter in the composition profiles due to the low number of ions in the nano-particles makes really difficult to assess the distribution of this element across the interface. These particles exhibited a carbon concentration close to the $Fe_8C$ structure reported for martensite in Fe-Ni-C alloys at the early stage of tempering

(40 ºC for 24 h) [33]. Although APT has the highest spatial resolution for compositional analysis, it does not provide information about the atomic configuration of these carbon-enriched regions. In the absence of any evidence to the contrary, it seems best to regard these regions as carbon atom clusters i.e., a preferential agglomeration of carbon atoms in the ferrite matrix.

ii) Particles with a carbon content of 17-26 at. % (Fig. 4), which might correspond to cementite or $Fe_4C$ carbon clusters with ~20 at. % C. Cementite particles ideally contain a carbon content of 25 at. %; however, an apparent low carbon concentration of cementite was reported in earlier atom probe studies [33,34]. This is due to the assignment of the carbon peak at a mass-to-charge state ratio of 12 Da to be exclusively $C^+$ rather than containing some $C_2^{++}$ ions, which will lead to a small underestimate of the true carbon level. However, all the particles detected with this level of carbon also show evidences of substitutional solute partitioning across the interface. The proximity histogram in Fig. 4 shows substitutional solute partitioning across the interface, but the trend for Mn seems opposite of what might be expected [24]. This additional information helps to discriminate between cementite and carbon clusters.

iii) Particles with a higher carbon content ranging from 27-30 at. % C (Fig. 5) were identified as ε-carbides. Chang and Smith [35] showed that ε-carbide precipitation did not accompany the partitioning of substitutional elements during the early stage of martensite tempering. In this work, all the particles detected with a carbon content of ~30 at.%, which is consistent with the carbides being ε-carbide, show some partitioning of substitutional solute elements such as Si across the interface.

As already mentioned, the initial carbide formed in lower bainite is generally accepted to be ε-carbide, which is subsequently replaced by cementite. In the present work, ε-carbide particles with a carbon content of 27-30 at. % C were only detected in the MC-LSi steel at 375 and 425 ºC using APT (Fig. 2). Moreover, cementite particles with a carbon content of 20-25 at. % C were identified at 375 and 400ºC in the same steel. Both type of particles showed clear evidence of substitutional solute partitioning across the interface at these transformation temperatures (375-425ºC). The extensive APT results presented herein failed to clearly detect ε-carbide in MC-HSi and HC-HSi steels transforming at temperatures lower than 375ºC.

Unfortunately, we are not able to discriminate between inter-lath cementite particles or intra-lath cementite particles using APT data. The fact that ε-carbide particles exist preferentially over cementite at higher temperatures for the MC-LSi steel suggested that the analysed cementite particles must be inter-lath cementite instead of lower bainite cementite. The rate at which the ε-carbide converts to cementite is expected to increase with temperature, but also depends on the starting steel composition. In fact, a high Si concentration retards the reaction, as is observed at all the temperature tested in the MC-HSi and HC-HSi steels in Fig. 2. These results are consistent with those widely reported for precipitation in martensite during tempering [8]. Bhadeshia and Edmonds [17] also failed to detect ε-carbide in high-silicon, medium-carbon steels, even during the early stages of the lower bainite transformation. The absence of partitioning of substitutional elements detected in the HC-HSi steel transformed at 300 ºC (full square symbol at 300 ºC in Fig. 2) suggests that cementite is originally formed by para-equilibrium growth. Eventually the substitutional elements will redistribute across the ferrite/cementite interface, as observed in most of the cases represented in Fig. 2.

Bhadeshia [36] explained the detection of cementite instead of ε-carbide in lower bainite in terms of carbon trapping at dislocations following the theory of tempering by Kalish and Cohen [21]. Carbon segregation at dislocations in the vicinity of the austenite-ferrite interface is another possible reaction that competes for carbon during carbide precipitation [31]. The detection of cementite as the transformation temperature decreased in Fig. 2 is consistent with the fact that the lower the reaction temperature, the higher the dislocation density in the bainitic ferrite [17,32]. The relatively high dislocation density associated with bainitic ferrite is often attributed to the plastic relaxation of the shape deformation accompanying the displacive transformation.

The average carbon levels of different Cottrell atmospheres detected by APT in the steels studied are listed in Table 4. Carbon trapped at dislocations was not observed in lower bainite in MC-LSi steel after extensive APT analysis (up to 26 specimens were tested). The amount of carbon segregated to dislocations, which were identified as carbon-enriched linear features, was estimated from APT using concentration profiles in a selected volume that included the feature, or using proximity histograms across that feature as Fig 6 illustrates. Other examples of carbon atom maps showing carbon segregation to dislocations in bainitic ferrite are reported elsewhere [37,38]. The range (7-16 at. %) for the amount of carbon trapped at dislocations shown in Table 4 is remarkable, and has no apparent correlation with the overall carbon content and the transformation temperature. Pereloma et al. [38] found by APT that the extent of solute segregation to a dislocation depends on its position relative to other defects. Consistent with this study, Cornide et al. [39] observed that dislocation tangles in the vicinity of the bainitic ferrite/austenite interface might trap higher amounts of carbon than single dislocations inside the bainitic ferrite lath. In addition, Cochardt et al. [40] pointed out

that the atmosphere around a screw dislocation can bind more than twice the number of carbon atoms associated with an edge atmosphere. Therefore, some significant variation in the carbon level at different dislocations or different segments of dislocations would be expected. Except in special cases [41], it is not possible to determine the type of dislocation observed by APT, as only the shape of, and the solute levels associated with, the observed atmosphere are revealed by this technique.

Beside the unclear trend of the segregation of carbon atoms to dislocations reported in Table 4 for high silicon steels as a function of temperature, these results suggest that the dislocation density in lower bainite could have an effect on the free energy of carbon in the bainitic ferrite, and hence could influence the carbide precipitation sequence, determining in particular where ε-carbide forms before the growth of cementite.

Carbon atom clusters, i.e., solute enriched regions with a carbon content of 11-16 at. % C and without evidence of substitutional solute partitioning, and represented in Fig. 2, were detected in the three steels at all the tested temperatures. These fluctuations in carbon concentration were repeatedly observed together with carbon segregation to dislocations during the earlier stage of tempering of the HC-HSi steel transformed at 200 ºC [23,24]. The nature of the carbon atom clustering processes seems to be associated with a redistribution of solute to lattice defects [42] and they might signify the onset of or precursors to carbide precipitation during the bainite reaction [43].

**Conclusions**

Atom probe tomography was used to determine the average carbon content of different features formed during the lower bainite reaction at different transformation

temperatures in three steels with different carbon and silicon contents. Based on their carbon contents, three different types of features were detected:

- Carbon clusters randomly dispersed throughout the bainitic ferrite matrix in the three steels at all the tested temperatures, with a carbon content of ~11 at. % and without evidence of substitutional solute partitioning. It is likely that these carbon-enriched regions may be associated with carbon segregation to lattice defects and may signify the onset of transitional carbide precipitation,
- ε-carbides exhibiting extensive substitutional solute partitioning, were only detected in lower bainitic microstructures formed at temperatures higher than 350 ºC in medium carbon low silicon steel. Complementary use of high resolution TEM will be required to confirm these particle identifications.
- Cementite instead of ε-carbide was observed in lower bainite formed bellow 350ºC in both high silicon steels studied.

Atom probe tomography evidence in high silicon steels suggest that dislocations in lower bainite trap substantial amount of carbon, and hence can influence the carbide precipitation sequence, determining in particular where ε-carbide forms before the growth of cementite.

**References**

[1] H.K.D.H Bhadeshia, J.W. Christian, Metall. Trans. A 21A (1990) 767-797.

[2] M. Takahashi, H.K.D.H. Bhadeshia, Mater. Sci. Technol. 6 (1990) 592-603.

[3] H.K.D.H. Bhadeshia, Acta Mater. 28 (1980) 1103-1114.

[4] L.C. Chang, Mater. Sci. Eng. A 368 (2004) 175-182.

[5] S.J. Matas, R.F. Hehemann, Trans. AIME 221 (1961) 179-185.

[6] E.C. Bain, Alloying Elements in Steel, American Society of Materials, Cleveland, 1939.

[7] G. Allten, P. Payson, Trans. ASM 45 (1953) 498–532.

[8] W.S. Owen, Trans. ASM 46 (1954) 812-829.

[9] S. Keh, W.C. Leslie, Materials Science Research, Vol. 1, Plenum Publishing, New York, 1963.

[10] J. Gordine, I. Codd, J. Iron Steel Inst. 207 (1969) 461–467.

[11] G.W. Lorimer, R.M. Hobbs, N. Ridley, J Iron Steel Inst. 210 (1972) 757–764.

[12] T. Sato, T. Nishizawa, J Jpn. Inst. Met. 19 (1955) 385-389.

[13] S.S. Babu, K. Hono, T. Sakurai, Metall. Mater. Trans. 25A (1994) 499-508.

[14] R.C. Thomson, M.K. Miller, Acta Mater. 46 (1998) 2203-2213.

[15] G. Miyamoto, T. Furuhara, T. Maki, J.C. Oh, K. Hono, in: J.M. Howe, D.E. Laughlin, J.K. Lee, U. Dahmen, W.A. Soffa (Eds), Proceedings of the solid-solid phase transformations in inorganic materials 2005. Vol. 1: Diffusional Transformations, John Wiley & Sons, London, 2005, pp 363-369.

[16] C.S. Roberts, B.L. Averbach, M. Cohen, Trans. ASM 45 (1957) 576-604.

[17] H.K.D.H. Bhadeshia, D.V. Edmonds, Metall. Trans. A 10 (1979) 895-907.

[18] E. Kozeschnik, H.K.D.H. Bhadeshia, Mater. Sci. Technol. 24 (2008) 343-347.

[19] R.W.K. Honeycombe, H.K.D.H. Bhadeshia, Steels: Microstructure and Properties, second ed, Butterworths–Hienemann, London, 1995.

[20] G. Ghosh, G.B. Olson, Acta Mater. 50 (2002) 2099-2119.

[21] D. Kalish, M. Cohen, Mater. Sci. Eng. 6 (1970) 156–166.

[22] T.D. Bigg, D.K. Matlock, J.G. Speer, D.V. Edmonds, Sol. St. Phen. 172-174 (2011) 827-832.

[23] F.G. Caballero, M.K. Miller, C. Garcia-Mateo, Metall. Mater. Trans. 42A (2011) 3660-3668.

[24] F.G. Caballero, M.K. Miller, C. Garcia-Mateo, C. Capdevila, S.S. Babu, Acta Mater. 56 (2008) 188-99.

[25] F.G. Caballero, M.J. Santofimia, C. Garcia-Mateo, C. Garcia de Andrés, Mater. T. JIM 45 (2004) 3272-3281.

[26] F.G. Caballero, M.J. Santofimia, C. García-Mateo, J. Chao, C. García de Andrés, Mater. Design 30 (2009) 2077-2083.

[27] F.G. Caballero, H.K.D.H. Bhadeshia, Curr. Opin. Solid State and Mater. Sci. 8 (2004) 251-257.

[28] C. Garcia de Andres, F.G. Caballero, C. Capdevila, L.F. Alvarez, Mater. Character. 46 (2001) 389-398.

[29] MK Miller, Atom Probe Tomography, Kluwer Academic/Plenum Press, New York, 2000.

[30] F.G. Caballero, M.K. Miller, C. Garcia-Mateo, J. Cornide, M.J. Santofimia, Scripta Mater. 67 (2012) 846–849.

[31] F.G. Caballero, M.K. Miller, S.S. Babu, C. Garcia-Mateo, Acta Mater. 55 (2007) 381-390.

[32] B.P.J. Sandvik, Metall. Trans. A 13 (1982) 777-787.

[33] M.K. Miller, P.A. Beaven, S.S. Brenner, G.D.W. Smith, Metall. Trans. A 14 (1983) 1021-1024.

[34] S.S. Babu, K. Hono, T. Sakurai, Metall. Mater. Trans. A 25: (1994) 499-508.

[35] L Chang, GDW Smith, J Phys 45-C9: (1984) 397-401.

[36] H.K.D.H. Bhadeshia, Mater. Sci. Technol. 5 (1989) 131-137.

[37] F.G. Caballero, H-W. Yen, M.K. Miller, J-R. Yang, J. Cornide, C. Garcia-Mateo, Acta Mater. 59 (2011) 6117-6123.

[38] E.V. Pereloma, I.B. Timokhina, J.J. Jonas, M.K. Miller, Acta Mater. 54 (2006) 4539-4551.

[39] J. Cornide, G. Miyamoto, F.G. Caballero, T. Furuhara, M.K. Miller, C. Garcia-Mateo, Solid State Phenom. 172-174 (2011) 117-122.

[40] A. Cochardt, G. Schoeck, H. Wiedersich, Acta Metall. 3 (1955) 533-537.

[41] D. Blavette, E. Cadel, A. Fraczkiewicz, A. Menand, Science 286 (1999) 2317-2319.

[42] M.K. Miller, P.A. Beaven, G.D.W. Smith, Metall. Trans. A 12 (1981) 1197-1204.

[43] K.A. Taylor, G.B. Olson, M. Cohen, J.B. Van der Sande, Metall. Trans. A 20 (1989) 2749-2765.

**Acknowledgement**

Research was supported by ORNL's Shared Research Equipment (ShaRE) User Facility, which is sponsored by the Office of Basic Energy Sciences, Scientific User Facilities Division, U.S. Department of Energy. The authors also gratefully acknowledge the support of the Research Fund for Coal and Steel (contract RFS-PR-11019) and the Spanish Ministry of Science and Innovation (contracts MAT2010-15330 and IPT-2012-0320-420000) for funding this research.

**Table Caption:**

Table 1: Chemical composition of studied steels, wt-%. The balance is Fe.

Table 2: Austenitisation conditions and experimental critical transformation temperatures

Table 3: Carbide distribution observed in the resultant bainitic microstructures

Table 4: Carbon trapped at dislocations determined by APT in high silicon steels

**Figure Captions:**

Fig. 1. Bright field TEM images of (a) upper bainite (i.e., bainitic ferrite and inter-lath carbide particles) obtained at 500 ºC for 1800 s in the MC-LSi steel; (b) lower bainite (i.e. bainitic ferrite and intra and inter-lath carbide particles) obtained at 375 ºC for 1800 s in the MC-LSi steel; (c) high silicon lower bainite (i.e., bainitic ferrite, intra-lath carbide and films of retained austenite) obtained at 375 ºC for 1100 s in the MC-HSi steel; (d) bainitic microstructure obtained at 250 ºC for 30 h in the HC-HSi steel; (e) dislocation debris in microstructure formed at 200 ºC for 10 days in the MC-HSi steel; $\alpha$ is bainitic ferrite and $\gamma$ is retained austenite. Arrows indicate the presence of carbide particles.

Fig. 2. Average carbon content estimated from APT data of different particles formed during lower bainite reaction at different temperatures and times long enough to ensure complete transformation in the studied steels (see Table 3 for details). Closed symbols indicate no distribution of substitutional elements across the ferrite/particle interface. Open symbols indicate partitioning of substitutional elements such as Si, Cr, and Mo across that interface. Solid horizontal lines delimitate the carbon content regime for clusters (7-16 at. % C).

Fig. 3. (a) Carbon isoconcentration surfaces at 2 at.% C superimposed with the carbon atom map, and (b) proximity histograms across carbon cluster in bainitic ferrite after transformation at 425 ºC for 1800 s in MC-LSi steel.

Fig. 4. (a) Carbon isoconcentration surfaces at 5 at.% C superimposed with the carbon atom map, (b) and (c) proximity histograms across cementite particle in bainitic ferrite after transformation at 400 ºC for 1800 s in MC-LSi steel.

Fig. 5. (a) Carbon isoconcentration surfaces at 5 at.% C superimposed with the carbon atom map, (b) and (c) proximity histograms across ε-carbide particle in bainitic ferrite after transformation at 425 ºC for 1800 s in MC-LSi steel.

Fig. 6. (a) Carbon atom map, (b) projected carbon atom map, and (c) proximity histograms across a dislocation in the vicinity of the bainitic ferrite/austenite interface in bainitic ferrite after transformation at 350 ºC for 1350 s in MC-HSi steel.

Table 1: Chemical composition of studied steels, wt-%. The balance is Fe.

| Steel | C | Si | Mn | Ni | Cr | Mo | V |
|---|---|---|---|---|---|---|---|
| MC-LSi | 0.30 | 0.25 | 1.22 | 0.10 | 0.14 | 0.03 | --- |
| (at. %) | (1.38) | (0.49) | (1.22) | (0.09) | (0.15) | (0.02) | |
| MC-HSi | 0.29 | 1.48 | 2.06 | --- | 0.43 | 0.27 | --- |
| (at. %) | (1.32) | (2.87) | (2.04) | | (0.45) | (0.15) | |
| HC-HSi | 0.98 | 1.46 | 1.89 | --- | 1.26 | 0.26 | 0.09 |
| (at. %) | (4.34) | (2.76) | (1.82) | | (1.28) | (0.14) | (0.09) |

Table 2: Austenitisation conditions and experimental critical transformation temperatures

| Steel | Austenitisation Conditions | $B_S$, ºC | $LB_S$, ºC | $M_S$, ºC |
|---|---|---|---|---|
| MC-LSi | 1200 ºC for 60 s | 525 ± 12 | 450 ± 12 | 342 ± 2 |
| MC-HSi | 925 ºC for 300 s | 450 ± 12 | 400 ± 12 | 299 ± 8 |
| HC-HSi | 1000 ºC for 900 s | 335 ± 12 | 335 ± 12 | 123 ± 4 |

$B_S$ bainite start, $LB_S$ lower bainite start and $M_S$ martensite start temperatures

Table 3: Carbide distribution observed in the resultant bainitic microstructures

| Steel | Bainite Transformation Temperature, ºC | Bainite Holding Time, s. | Carbide distribution |
|---|---|---|---|
| MC-LSi | 525 | 1,800 | Inter-lath |
| | 500 | 1,800 | Inter-lath |
| | 475 | 1,800 | Inter-lath |
| | $LB_S$=450 ºC | | Mixed* |
| | 425 | 1,800 | Intra and Inter-lath |
| | 400 | 1,800 | Intra and Inter-lath |
| | 375 | 1,800 | Intra and Inter-lath |
| MC-HSi | 425 | 1,000 | Carbide-free |
| | $LB_S$=400 ºC | | Mixed* |
| | 375 | 1,100 | Intra-lath |
| | 350 | 1,350 | Intra-lath |
| | 325 | 1,350 | Intra-lath |
| HC-HSi | 300 | 43,200 (12 hours) | Intra-lath |
| | 250 | 108,000 (30 hours) | Intra-lath |
| | 200 | 864,000 (10 days) | Intra-lath |

*The observation of inter- and intra-lath carbide distributions allowed defining the lower bainite start ($LB_S$) temperature.

Table 4: Carbon trapped at dislocations determined by APT in high silicon steels

| Steel | Transformation temperature, ºC | Carbon in Cottrell atmosphere, at.% |
|---|---|---|
| MC-HSi | 350 | 12.2±0.4 |
| | | 9.6±2.9 |
| | | 14.4±2.9 |
| | | 13.0±1.7 |
| | | 16.3±2.9 |
| HC-HSi | 200 | 14.0 ±2.2 |
| | | 7.4 ± 0.1 |
| | | 7.4 ± 2.6 |
| | | 5.8 ±3.0 |
| | | 13.4 ± 0.8 |

† Error bars representing the statistical scatter in the APT composition profiles due to the number of ions in each slice of the selected volume of analysis.

**Table Captions:**

Table 1: Chemical composition of studied steels, wt-%. The balance is Fe.

Table 2: Austenitisation conditions and experimental critical transformation temperatures

Table 3: Carbide distribution observed in the resultant bainitic microstructures

Table 4: Carbon trapped at dislocations determined by APT in high silicon steels

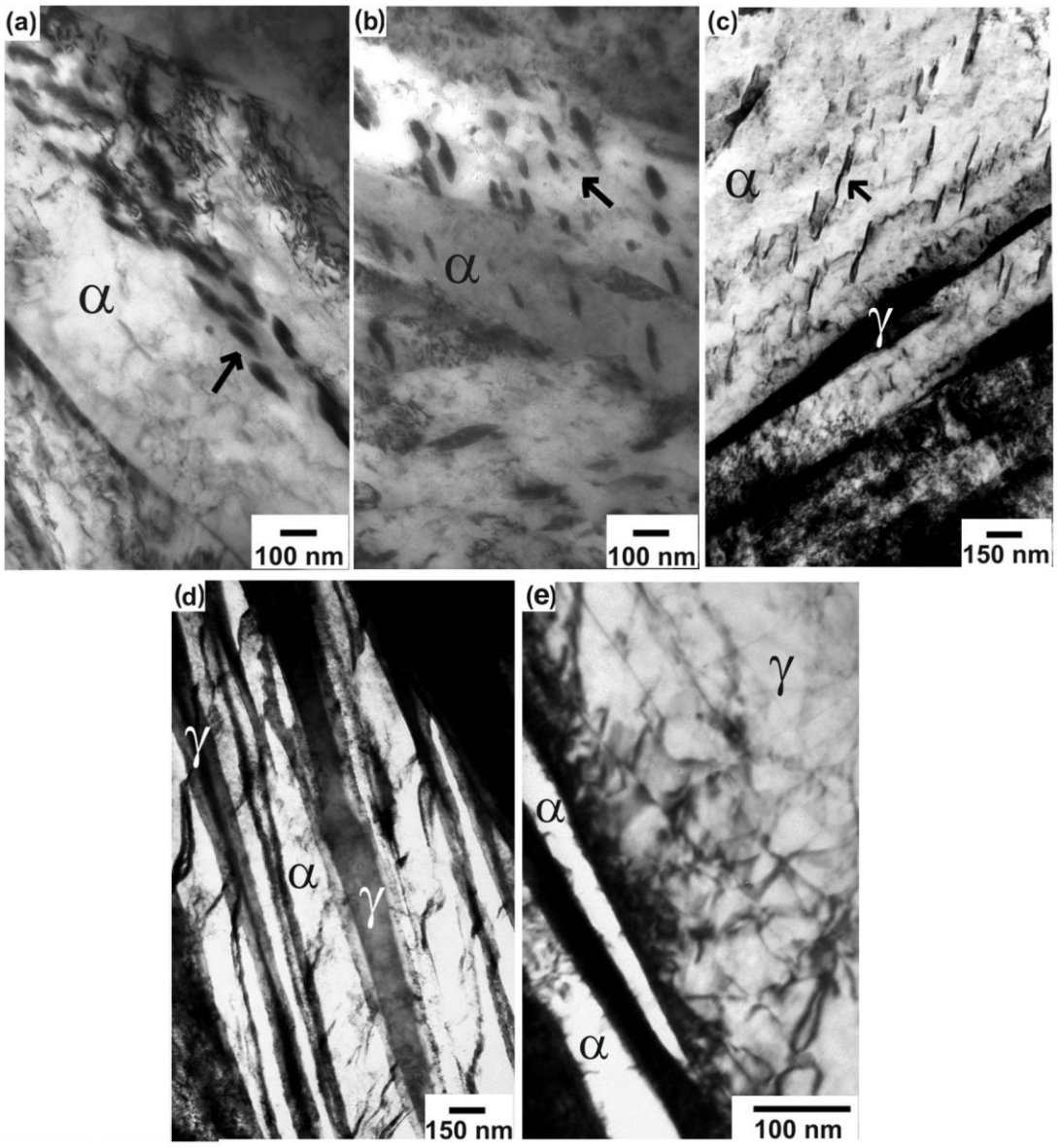


Fig. 1. Bright field TEM images of (a) upper bainite (i.e., bainitic ferrite and inter-lath carbide particles) obtained at 500 ºC for 1800 s in the MC-LSi steel; (b) lower bainite (i.e. bainitic ferrite and intra and inter-lath carbide particles) obtained at 375 ºC for 1800 s in the MC-LSi steel; (c) high silicon lower bainite (i.e., bainitic ferrite, intra-lath carbide and films of retained austenite) obtained at 375 ºC for 1100 s in the MC-HSi steel; (d) bainitic microstructure obtained at 250 ºC for 30 h in the HC-HSi steel; (e) dislocation debris in microstructure formed at 200 ºC for 10 days in the MC-HSi steel;

$\alpha$ is bainitic ferrite and $\gamma$ is retained austenite. Arrows indicate the presence of carbide particles.

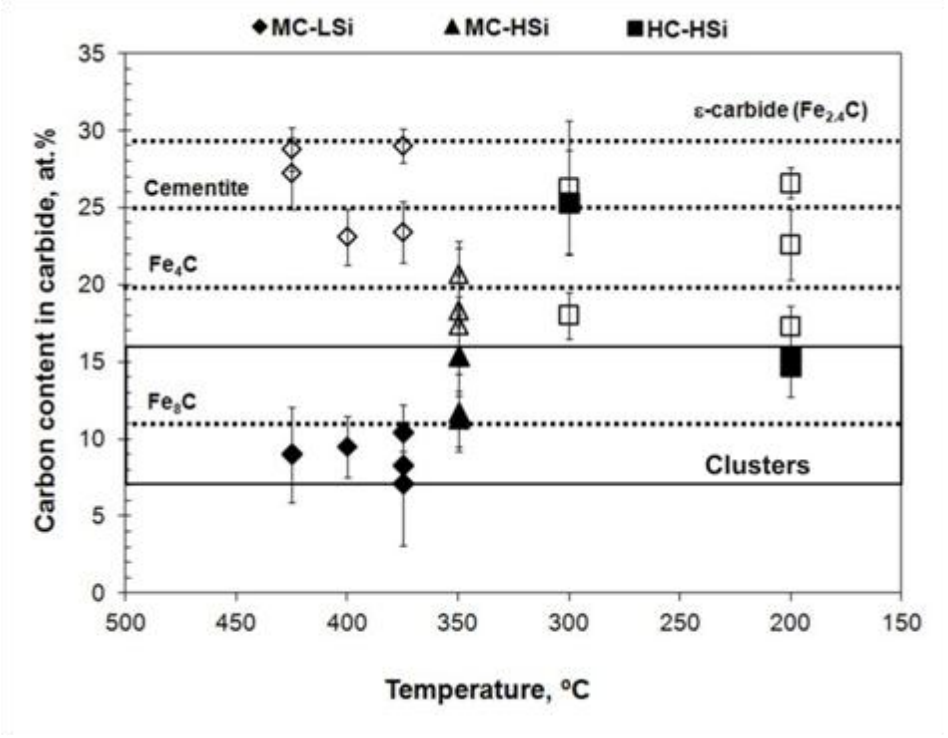


Fig. 2. Average carbon content estimated from APT data of different particles formed during lower bainite reaction at different temperatures and times long enough to ensure complete transformation in the studied steels (see Table 3 for details).. Closed symbols indicate no distribution of substitutional elements across the ferrite/particle interface. Open symbols indicate partitioning of substitutional elements such as Si, Cr, and Mo across that interface. Solid horizontal lines delimitate the carbon content regime for clusters (7-16 at. % C).

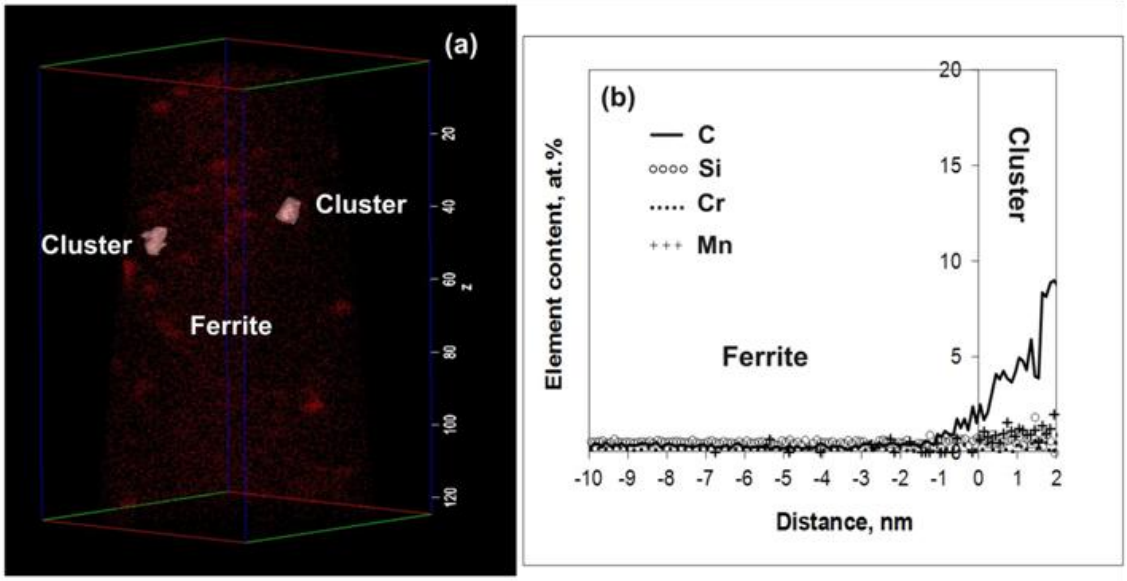


Fig. 3. (a) Carbon isoconcentration surfaces at 2 at.% C superimposed with the carbon atom map, and (b) proximity histograms across carbon cluster in bainitic ferrite after transformation at 425 ºC for 1800 s in MC-LSi steel.

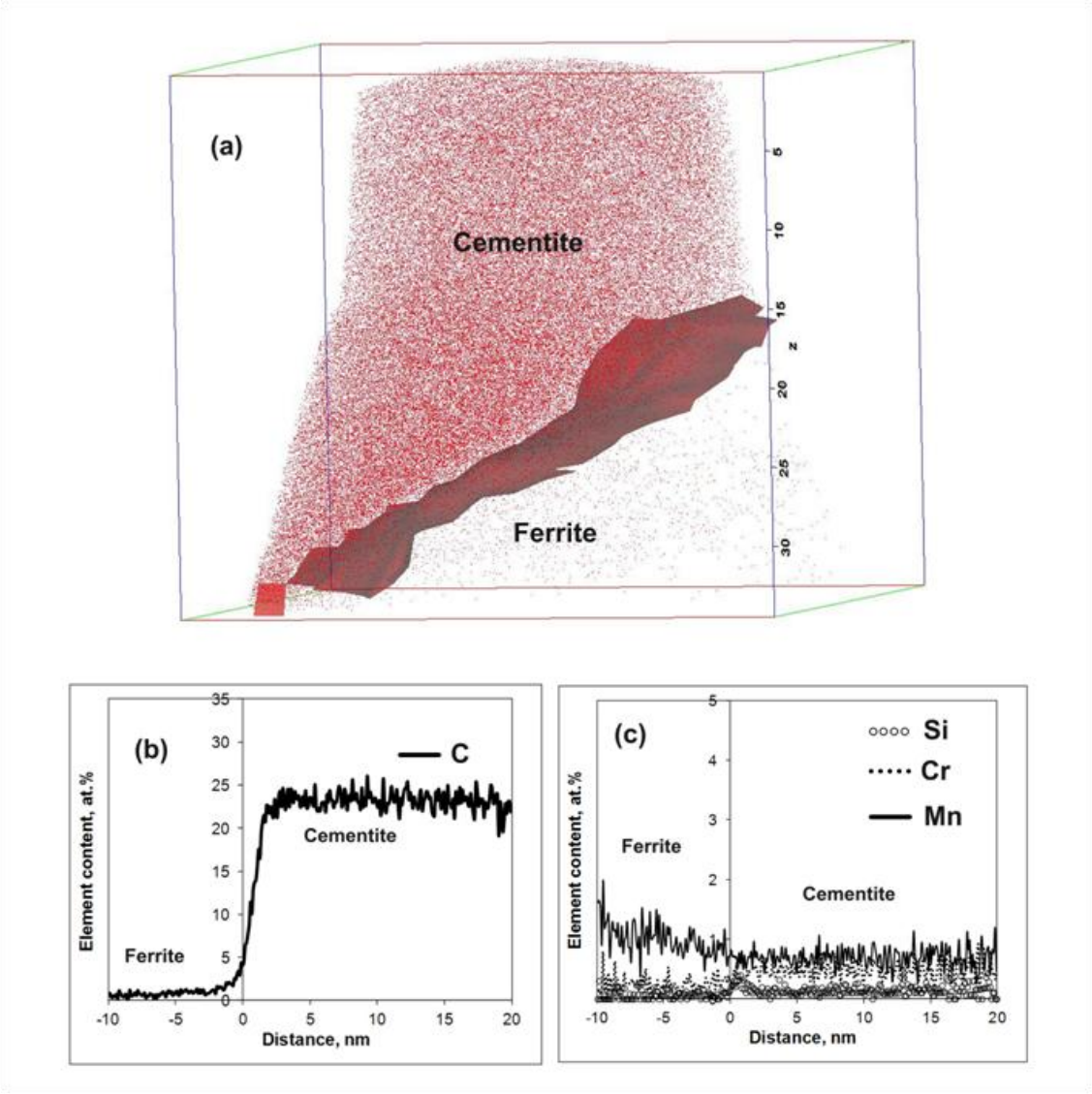


Fig. 4. (a) Carbon isoconcentration surfaces at 5 at.% C superimposed with the carbon atom map, (b) and (c) proximity histograms across cementite particle in bainitic ferrite after transformation at 400 ºC for 1800 s in MC-LSi steel.

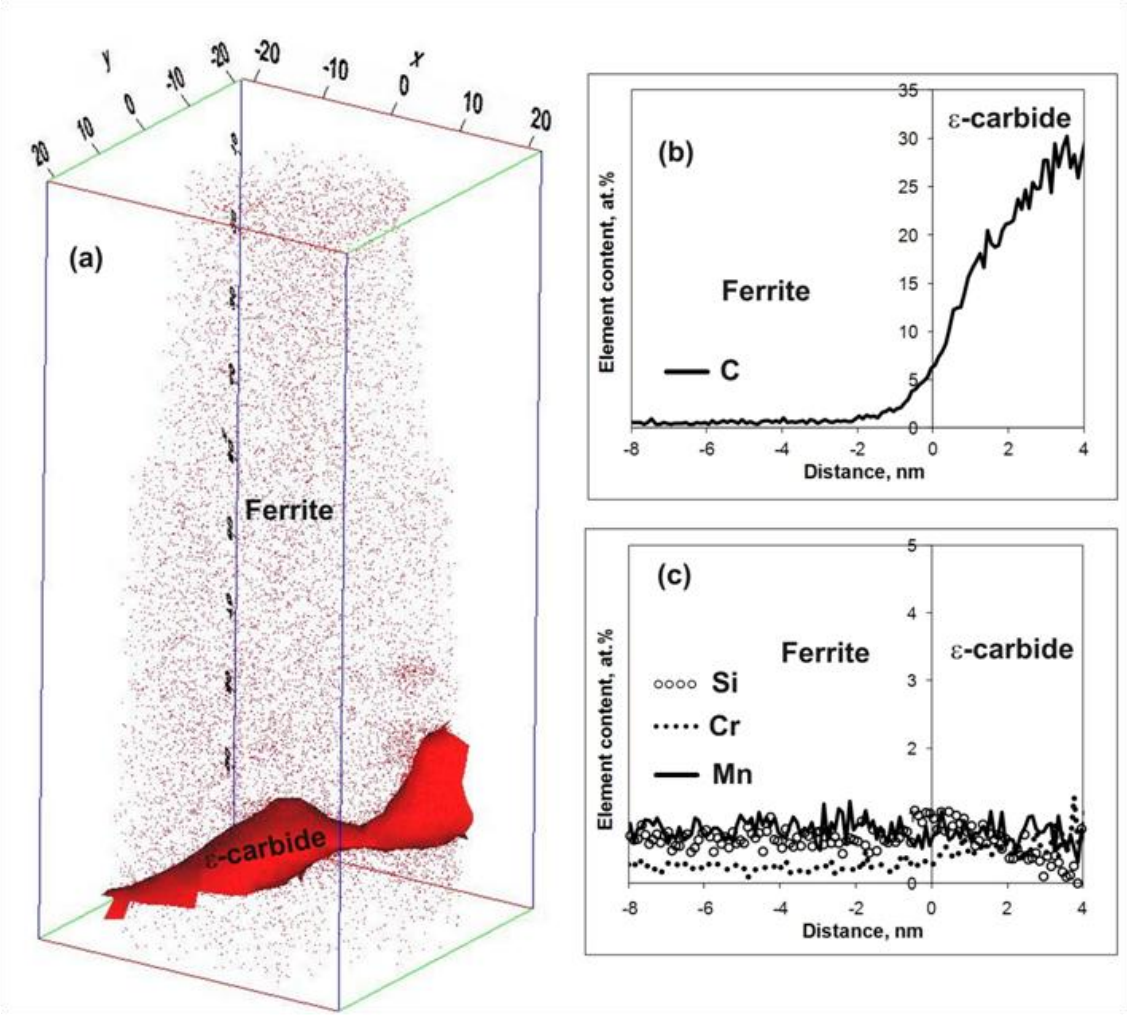


Fig. 5. (a) Carbon isoconcentration surfaces at 5 at.% C superimposed with the carbon atom map, (b) and (c) proximity histograms across ε-carbide particle in bainitic ferrite after transformation at 425 ºC for 1800 s in MC-LSi steel.

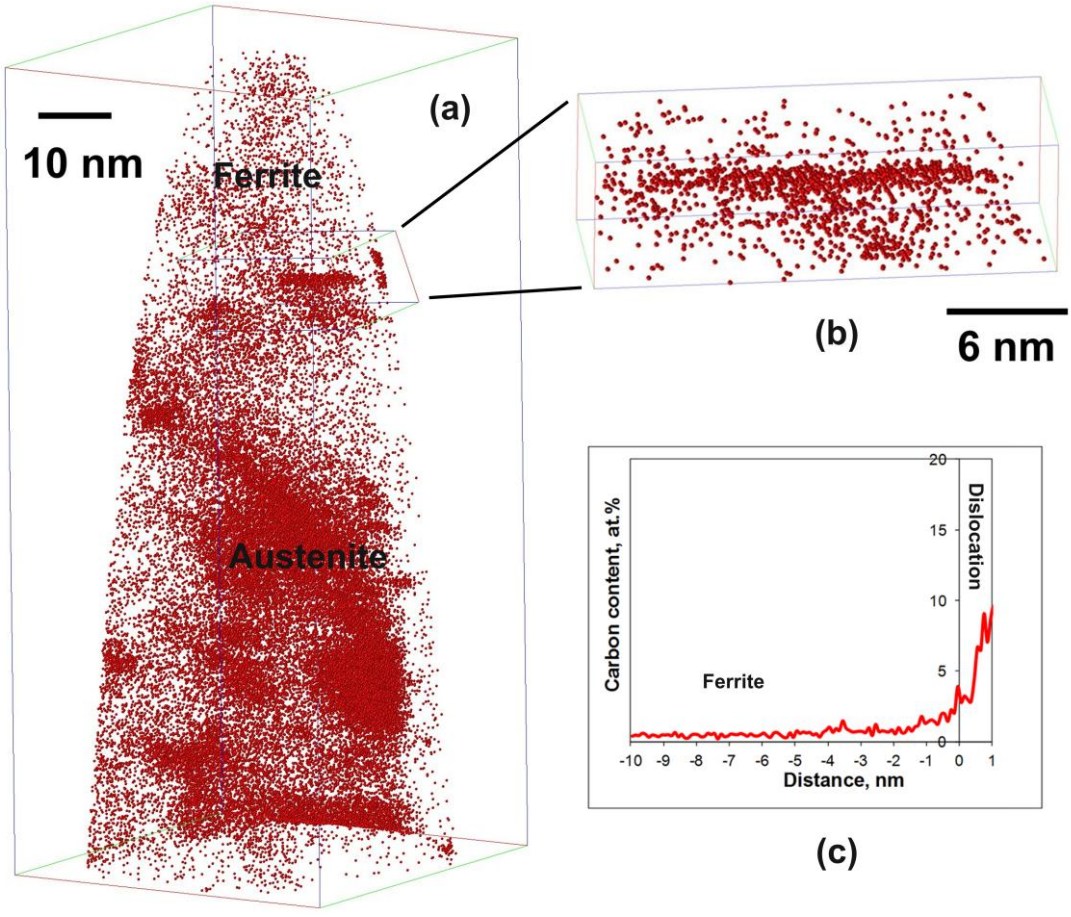


Fig. 6. (a) Carbon atom map, (b) projected carbon atom map, and (c) proximity histograms across a dislocation in the vicinity of the bainitic ferrite/austenite interface in bainitic ferrite after transformation at 350 ºC for 1350 s in MC-HSi steel.